

ARTICLE

DOI: 10.1038/s41467-018-04994-z

OPEN

TGF- β signaling alters H4K20me3 status via miR-29 and contributes to cellular senescence and cardiac aging

Guoliang Lyu¹, Yiting Guan¹, Chao Zhang¹, Le Zong¹, Lei Sun¹, Xiaoke Huang¹, Li Huang¹, Lijun Zhang¹, Xiao-Li Tian², Zhongjun Zhou^{3,4} & Wei Tao¹

Cellular senescence is a well-orchestrated programmed process involved in age-related pathologies, tumor suppression and embryonic development. TGF- β /Smad is one of the predominant pathways that regulate damage-induced and developmentally programmed senescence. Here we show that canonical TGF- β signaling promotes senescence via miR-29-induced loss of H4K20me3. Mechanistically, oxidative stress triggers TGF- β signaling. Activated TGF- β signaling gives rise to acute accumulation of miR-29a and miR-29c, both of which directly suppress their novel target, Suv4-20h, thus reducing H4K20me3 abundance in a Smad-dependent manner, which compromises DNA damage repair and genome maintenance. Loss of H4K20me3 mediated by the senescent TGF- β /miR-29 pathway contributes to cardiac aging *in vivo*. Disruption of TGF- β signaling restores H4K20me3 and improves cardiac function in aged mice. Our study highlights the sequential mechanisms underlying the regulation of senescence, from senescence-inducing triggers to activation of responsive signaling followed by specific epigenetic alterations, shedding light on potential therapeutic interventions in cardiac aging.

¹The MOE Key Laboratory of Cell Proliferation and Differentiation, School of Life Sciences, Peking University, Beijing 100871, China. ²Department of Human Population Genetics, Human Aging Research Institute and School of Life Science, Nanchang University, Nanchang 330031, China. ³School of Biomedical Sciences, LKS Faculty of Medicine, The University of Hong Kong, 21 Sassoon Road, Hong Kong, China. ⁴Shenzhen Institute of Innovation and Research, The University of Hong Kong, Nanshan, Shenzhen 518000, China. These authors contributed equally: Guoliang Lyu, Yiting Guan. Correspondence and requests for materials should be addressed to W.T. (email: weitao@pku.edu.cn)

Cellular senescence is featured by a state of cell proliferation arrest, accumulation of senescence-associated β -galactosidase (SA- β -gal)¹, emergence of senescence-associated secretory phenotypes (SASP)² and expression of cyclin-dependent kinase inhibitors (CKIs)^{3,4}. Cellular senescence is triggered by a myriad of extracellular and intracellular stimuli^{5–7}, and it is involved, pathologically or physiologically, in age-related disorders, tumor suppression and tissue patterning^{8–10}. The process of senescence is coordinated through a variety of regulatory networks directed by endogenous and exogenous senescence-inducing signals^{11,12}.

TGF- β /Smad signaling is one of the prominent pathways regulating both damage-induced senescence and developmentally programmed senescence¹³. The pathway is evolutionarily conserved and participates in an enormous range of biological processes that influence various physiological activities, including cell cycle control, wound healing, bone morphogenesis, carcinogenesis, tumor suppression and differentiation in cell-type specific and context-dependent manners^{14–16}. Upon binding of TGF- β , the type II (T β R2) and type I receptor (T β R1) kinases undergo a series of complex formation and phosphorylation events, leading to activation of T β R1, followed by signal transduction via the formation of complexes comprising phosphorylated receptor-regulated pSmad2/3 and the common mediator Smad4. Next, the Smad complex is translocated into the nucleus, where it regulates transcription of downstream target genes through physical interaction and functional cooperation with other co-factors¹⁷. In vivo and in vitro models have confirmed that TGF- β signaling, activated by SASP or other developmental cues, regulates senescence via up-regulation of p15 and/or p21 in damage-induced and developmental senescence¹⁸. These findings indicate that TGF- β pathway plays an important role in senescence as one of the key sensors mediating senescent signaling in response to environmental stresses and endogenous signals.

Epigenetic programming in the forms of DNA methylation patterns^{19,20}, histone modification landscapes^{21–23}, chromatin architecture organization^{24,25} and non-coding RNAs^{26,27} contributes to senescence and is widely accepted as a hallmark of senescence. Epigenetic alterations influence senescence by impinging on DNA damage repair, telomere length and metabolic pathways²⁸, or activating expression of senescence-related genes and miRNAs^{29,30}. Multiple lines of evidence suggest that alterations of chromatin states are closely linked to the control of cellular senescence^{31–33}. Cells can sense diverse senescence-inducing stimuli, which activate signaling pathways that drive changes in chromatin status^{34,35}. However, the pathways through which senescence signals cause such alterations remain largely unknown.

In this study, we report that TGF- β /Smad signaling triggers miR-29-mediated reduction of H4K20me3 abundance, which promotes cellular senescence. We demonstrate a sequential regulatory axis, in which H4K20me3, as a responsive downstream epigenetic effector of the TGF- β /Smad pathway, is negatively regulated by miR-29 to regulate cellular senescence. Disruption of TGF- β signaling restores global H4K20me3 abundance in the aged murine heart and partially improves cardiac function in vitro. Our study reveals an epigenetics-based responsive pathway that drives alterations in histone modification status during cellular senescence.

Results

miR-29-mediated loss of H4K20me3 promotes senescence. To examine senescence-associated changes of histone modifications, we performed histone modifications scanning in senescent cells. The results showed that H4K20me1, -me2, and -me3 exhibited

prominent down-regulation in senescent mouse embryonic fibroblasts (MEFs) (Fig. 1a; Supplementary Fig. 1a–c). Accordingly, the expression levels of Suv4-20h1 and Suv4-20h2, the two major methyltransferases mediating H4K20me3, were also decreased during senescence (Fig. 1b–d). Furthermore, depletion of Suv4-20h1, Suv4-20h2 or both (designated as Suv4-20h) by shRNAs and treatment with selective Suv4-20h inhibitor A-196³⁶ led to reduced H4K20me3 protein abundance and premature senescence (Fig. 1e–j and Supplementary Fig. 1d–k), consistent with a previous finding that knockout of *Suv4-20h1* and *Suv4-20h2* contributed to defective proliferation and cell cycle progression in MEFs³⁷. These results suggest that H4K20me3 is a negative regulator of senescence.

Next, we looked into the mechanisms underlying the cellular alterations described above. miRNAs can silence gene expression via mRNA destabilization and/or translational repression³⁸, so we reasoned that Suv4-20h silencing might be caused by miRNAs. Through bioinformatics analyses via TargetScan, PicTar and miRDB^{39–41}, we identified three putative miRNAs targeting miRNA response elements (MREs) residing in 3' untranslated region (3' UTR) of *Suv4-20h1* mRNA: miR-29a-3p, miR-29b-3p and miR-29c-3p (denoted as miR-29a, miR-29b and miR-29c, respectively). The three miRNAs belong to the miR-29 family and function in a synergistic manner in a wide range of physiological activities^{42–44}. It is likely that miR-29a, miR-29b and miR-29c target the 3' UTRs of *Suv4-20h1* and *Suv4-20h2* via incomplete complementary binding to their potential MREs (Supplementary Fig. 2a). Apart from miR-29, three other miRNAs, miR-125a-5p, miR-125b-5p and miR-24-3p, were predicted to target the 3' UTR of *Suv4-20h2* (Supplementary Fig. 2b, c). To validate whether Suv4-20h1 and Suv4-20h2 are bona fide targets of the predicted miRNAs, we generated luciferase reporter constructs, in which the 3' UTR of *Suv4-20h* was placed behind the luciferase gene. As shown in Supplementary Fig. 2d,e, the luciferase activity assay indicated that miR-29 targeted the 3' UTR of *Suv4-20h*, but miR-125a-3p, miR-125b-3p and miR-24-3p did not. The inhibitory effects were attenuated when the miR-29 binding sites on the MREs were mutated (Fig. 2a, b). Furthermore, forced expression or inhibition of miR-29, by individual transfection of miRNA mimics (M-miR-29) or inhibitors (I-miR-29a and I-miR-29c), resulted in decreased or increased H4K20me3 abundance, respectively (Fig. 2c and Supplementary Fig. 2f–l). Gain of function of miR-29 via lentiviral infection led to reduced protein levels of Suv4-20h and H4K20me3 (Fig. 2d and Supplementary Fig. 2m). These results indicate that Suv4-20h1 and Suv4-20h2 are novel direct targets of miR-29.

To investigate the role of miR-29 in senescence, we performed differential miRNA expression analyses in serially passaged MEFs, which revealed accumulation of miR-29a and miR-29c, but nearly unaltered abundance of miR-29b, in senescent cells (Supplementary Fig. 2n, o). Increased abundance of miR-29 (represented miR-29a and miR-29c hereinafter) in early passaged cells (PD4) accelerated senescence whereas decreased amounts of miR-29 in late passaged cells (PD8) delayed senescent phenotypes (Fig. 2e–g and Supplementary Fig. 2p). Moreover, re-introducing 3' UTR-depleted *Suv4-20h1* and *Suv4-20h2* alleviated the miR-29-induced reduction in H4K20me3 abundance (Fig. 2h and Supplementary Fig. 2q, r) and inhibition of senescence progression (Fig. 2i, j and Supplementary Fig. 2s). Taken together, these results suggest that miR-29 directly suppresses Suv4-20h through incomplete complementarity to MREs in the 3' UTR of *Suv4-20h* to promote cellular senescence.

TGF- β signaling regulates expression of miR-29. Next we explored the manner in which miR-29 expression is regulated during cellular senescence. The TGF- β /Smad pathway participates

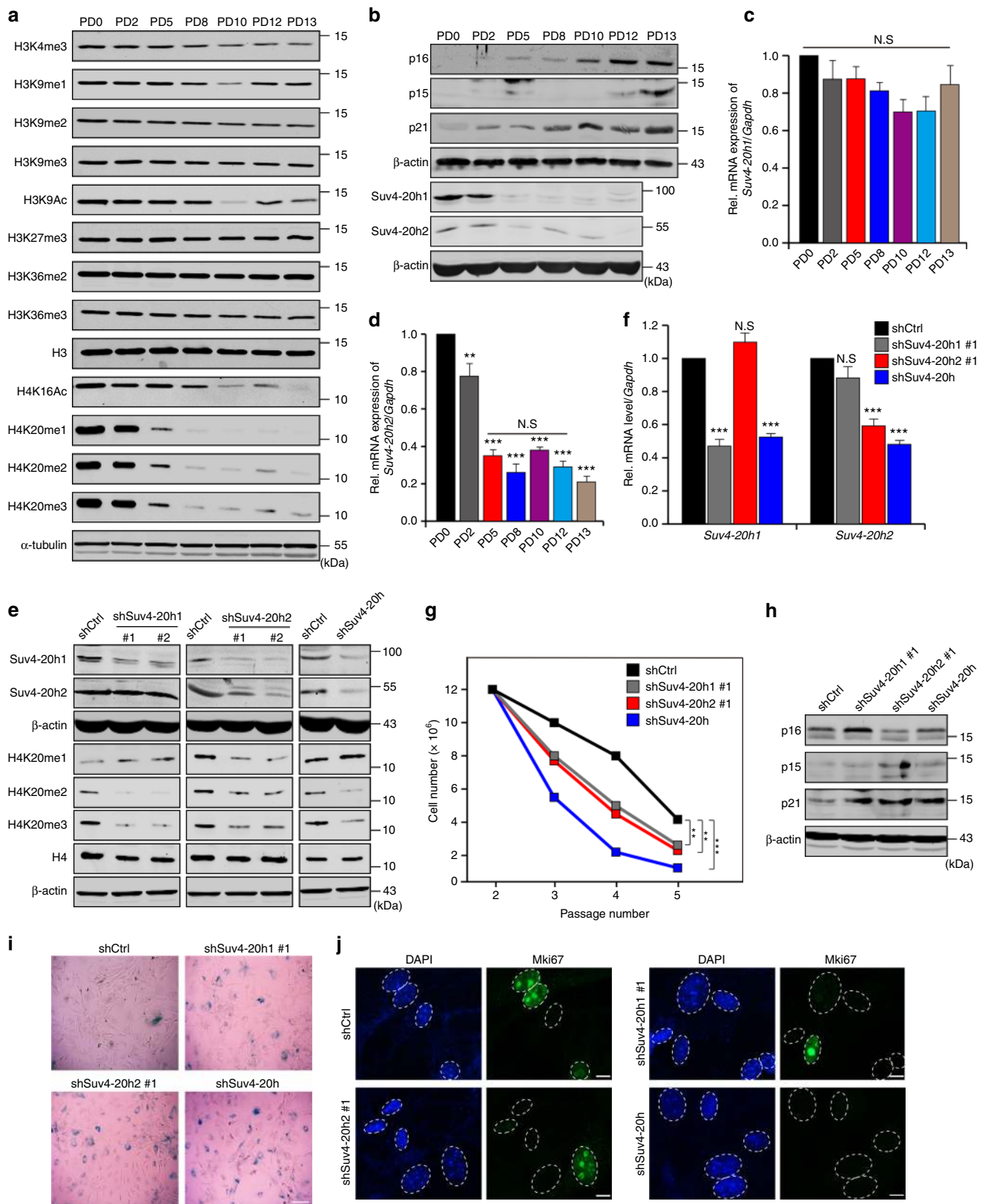
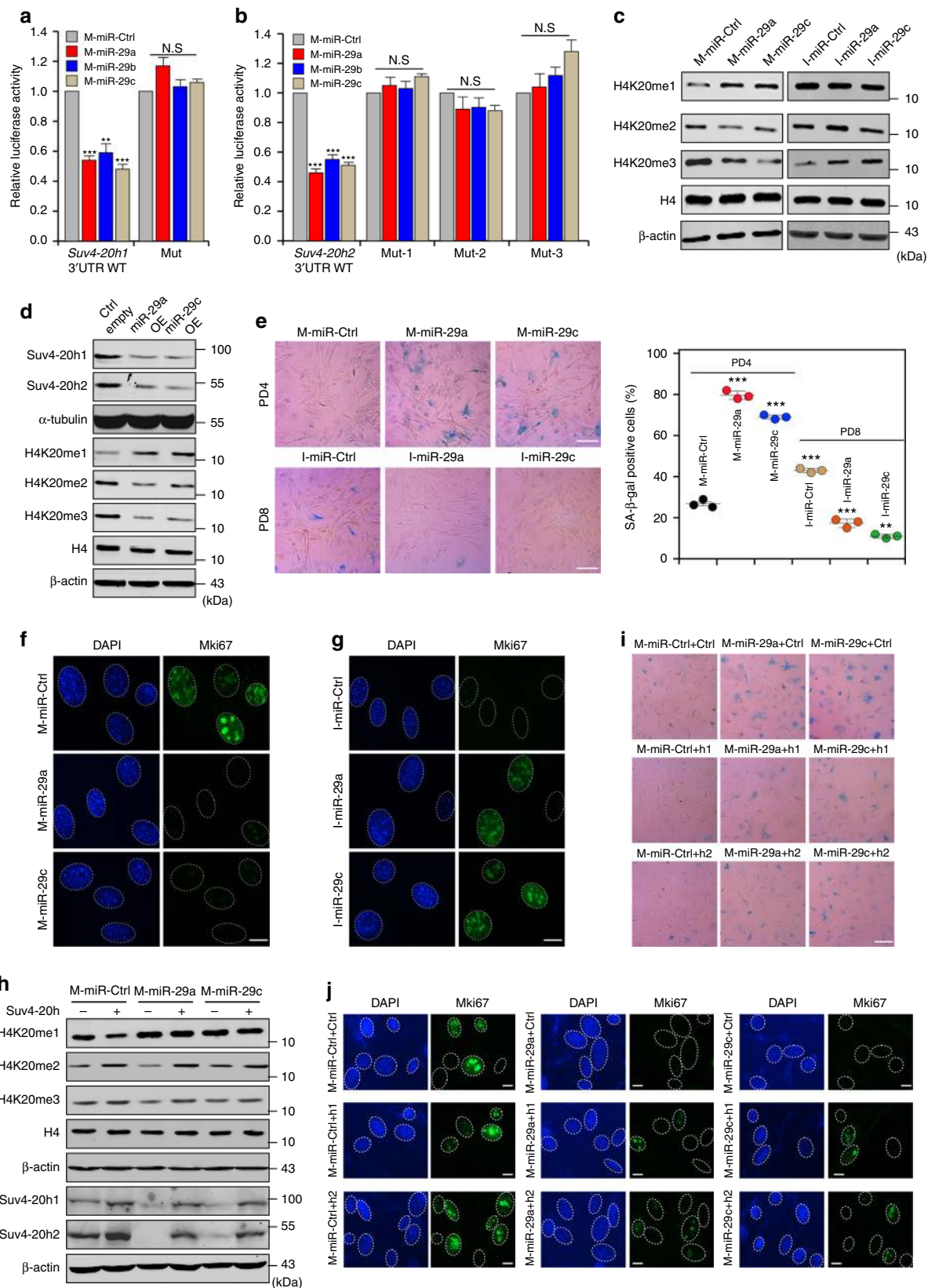


Fig. 1 Loss of H4K20me3 promotes cellular senescence. **a** Western blot for total protein of the indicated histone modifications from serially passaged MEFs. H3, H4 and α -tubulin served as loading controls. **b** Western blots showing expression of p16, p15, p21, Suv4-20h1 and Suv4-20h2 during MEFs senescence. β -actin served as a loading control. **c**, **d** Real-time qPCR analysis of *Suv4-20h1* (**c**) and *Suv4-20h2* (**d**) mRNA expression in different passages of MEFs. **e**, **f** Western blot (**e**) and RT-qPCR (**f**) for Suv4-20h in knockdown cells. **g** Growth curve of Suv4-20h-depleted cells. **h** Expression of p16, p15 and p21 in Suv4-20h knockdown cells. β -actin served as a loading control. **i** SA- β -gal staining in control (Ctrl) and Suv4-20h (shSuv4-20h) knockdown cells. Scale bar, 20 μ m. **j** Immunofluorescent staining of Mki67 in control (Ctrl) and Suv4-20h depleted cells. Scale bar, 5 μ m. Two-tailed unpaired Student *t*-tests were performed, ***p* < 0.01, ****p* < 0.001

in the regulation of transcription or processing of miRNA in human/mouse endothelial cells⁴⁵ and human primary pulmonary artery smooth muscle cells (PASMCs)⁴⁶. We examined whether TGF- β signaling regulates biogenesis of miR-29 during MEFs

senescence. Levels of primary miR-29 (pri-miR-29) and mature miR-29 were measured when canonical TGF- β signaling was either activated by TGF- β or abolished by E-616452, a TGF- β signaling inhibitor. Expression levels of pri-miR-29 and miR-29



were elevated upon activation of TGF- β signaling (Supplementary Fig. 3a), whereas their levels were decreased in the presence of E-616452 (Fig. 3a, b), suggesting that TGF- β signaling positively regulates transcription of miR-29.

Next, we assessed the impact of Smad4, a common downstream effector of TGF- β signaling, on transcription of *Mir29a* and *Mir29c*. Knockout or knockdown of *Smad4* (Smad4KO or shSmad4) reduced the abundance of pri-miR-29 and miR-29 (Fig. 3c, d and Supplementary Fig. 3b–e). Promoter luciferase reporter assays indicated increased luciferase activity in cells with ectopic expression of Smad4 and the fused reporter constructs containing predicted promoters of *Mir29a/c* upstream of the luciferase gene, in comparison with cells treated with the control vector (Supplementary Fig. 3f). Chromatin immunoprecipitation (ChIP) with Smad4 antibodies followed by qPCR indicated that Smad4 directly bound to upstream sequences harboring the Smad binding elements (SBEs) of *Mir29a* and *Mir29c* (Fig. 3e, f and Supplementary Fig. 3g, h). In addition, suppressing TGF- β signaling by inhibitor treatment or *Smad4* knockout impaired Smad4 enrichment on the SBEs of *Mir29a* and *Mir29c* (Fig. 3g, h), which suggests that Smad4 is involved in TGF- β -regulated transcriptional up-regulation of miR-29 in senescent MEFs. Meanwhile, disruption of the TGF- β pathway by E-616452 treatment mitigated the increase in miR-29 abundance (Fig. 3i and Supplementary Fig. 3i) and progression of senescence in cells with ectopic miR-29 (Fig. 3j, k and Supplementary Fig. 3j). Together, these results demonstrate that TGF- β signaling activates miR-29 expression in a Smad-dependent manner.

TGF- β signaling accelerates senescence via miR-29/H4K20me3.

Given that TGF- β signaling controls expression of miR-29, which represses H4K20me3 by inhibiting Suv4-20h, we tested whether activated TGF- β signaling expedites senescence by reducing the abundance of H4K20me3. We cultured cells in physiological (3%) oxygen (physioxia) and atmospheric (20%) oxygen (relative hyperoxia), because previous findings revealed that hyperoxia-induced oxidative stress activated the TGF- β pathway and accelerated senescence^{47,48}. Indeed, compared to physioxia, hyperoxia promoted senescence and triggered activation of TGF- β signaling (Supplementary Fig. 4 and Fig. 4a). Activation of TGF- β signaling by oxidative stress was accompanied by increased miR-29 accumulation (Fig. 4b, c) and accelerated reduction in the abundance of total H4K20me3 (Fig. 4d).

Furthermore, inhibition of TGF- β signaling by inhibitor treatment and Smad4 depletion diminished miR-29 expression, attenuated the reduction in Suv4-20h1 and Suv4-20h2 expression and produced partial recovery of H4K20me3 (Fig. 4e and Supplementary Fig. 5a–c). Moreover, alterations in TGF- β signaling changed the progression of senescence and specifically altered H4K20me3 without affecting other histone modifications (Supplementary Fig. 5d–h). Disruption of TGF- β signaling by E-

616452 restored H4K20me3 levels (Fig. 4f), attenuated SA- β -gal staining and enhanced the Mki67 signals (Fig. 4g, h) in Suv4-20h-depleted cells, suggesting that H4K20me3 is a downstream effector of TGF- β signaling. In addition, after miR-29 was destroyed by miRNA inhibitors, activation of TGF- β signaling did not down-regulate Suv4-20h and H4K20me3 (Fig. 4i). Collectively, these data demonstrate that TGF- β accelerates cellular senescence by facilitating the miR-29-mediated loss of H4K20me3.

Reduction of H4K20me3 causes defective DNA damage repair.

H4K20me3 contributes to the processes of DNA damage repair and genomic maintenance^{49–51}. We evaluated the role of TGF- β -miR-29 axis-regulated inhibition of H4K20me3 and DNA damage repair in senescent process. Inhibition of TGF- β signaling increased the fluorescent signals and/or protein levels of γ H2AX and 53BP1 (Fig. 5a–d and Supplementary Fig. 6a–e), indicating that TGF- β signaling suppresses DNA damage repair in senescent cells. To investigate whether compromised DNA damage repair is a consequence of the global loss of H4K20me3, acute DNA damage was introduced by etoposide treatment for two hours. DNA damage repair was examined by measuring γ H2AX and 53BP1 signals on the indicated time-course after the etoposide treatment was ceased. Suv4-20h2-depleted and Suv4-20h inhibitor-treated cells showed decreased global γ H2AX protein abundance, prolonged persistence of γ H2AX level and severe loss of 53BP1 after etoposide treatment (Fig. 5e and Supplementary Fig. 6f–h). These results indicate that H4K20me3 protects DNA from damage by facilitating DNA repair involving 53BP1.

To further substantiate whether TGF- β signaling compromises DNA damage repair and genomic maintenance by reducing the abundance of H4K20me3, the chromatin structures of normal cells and Suv4-20h knockdown cells, were analyzed by micrococcal nuclease (MNase) sensitivity assays in the presence and absence of E-616452. Activation of TGF- β signaling increased MNase sensitivity, while inhibition of TGF- β signaling decreased MNase accessibility (Fig. 5f–j). Moreover, inhibition of TGF- β signaling moderately attenuated MNase sensitivity in Suv4-20h-depleted cells (Supplementary Fig. 6i–k). The clonogenic cell survival assays utilizing HEK293T cells demonstrated that losing *SUV4-20H* conferred increased sensitivity to DNA damage because the abundance of H4K20me3 was reduced (Fig. 5k and Supplementary Fig. 6l, m). Taken together, these results suggest that TGF- β signaling delays DNA damage repair and impairs genomic maintenance by ablating H4K20me3.

TGF- β /miR-29 signaling is involved in cardiac dysfunctions.

Given that cellular senescence may accelerate aging when tissues exhaust their regenerative capacity^{52–54}, and the TGF- β /Smad pathway participates in programmed senescence during tissue development, we investigated whether TGF- β -miR-29 signaling

Fig. 2 miR-29-mediated reduction of H4K20me3 leads to premature cellular senescence. **a, b** Luciferase assays with the wild-type *Suv4-20h1* 3' UTR or mutated *Suv4-20h1* 3' UTR (**a**), as well as with the wild-type *Suv4-20h2* 3' UTR or mutated *Suv4-20h2* 3' UTR (**b**) in the predicted binding site of miR-29a, miR-29b and miR-29c, transfected with control miRNA mimics (M-miR-Ctrl) or miR-29 mimics (M-miR-29a, M-miR-29b and M-miR-29c). **c** Protein levels of H4K20 were measured by western blotting in MEFs transfected with M-miR-29 or miR-29 inhibitors (I-miR-29a and I-miR-29c). β -actin served as a loading control. **d** Western blot for global H4K20 methylation in cells with lentivirus-mediated ectopic expression of the indicated miR-29. β -actin served as a loading control. **e** SA- β -gal staining and diagrams showing MEFs from PD4 transfected with M-miR-29 and MEFs from PD8 transfected with I-miR-29. Scale bar, 20 μ m. One-way ANOVA with Dunnett's multiple comparison test was performed. **f, g** Immunofluorescent staining of Mki67 in MEFs transfected with M-miR-29 (**f**) or I-miR-29 (**g**). Scale bar, 5 μ m. **h** Cells were first transfected with M-miR-Ctrl, M-miR-29a or M-miR-29c, after which they were infected with pBabe, pBabe-Suv4-20h1 or pBabe-Suv4-20h2 and subjected to western blotting for the indicated protein. β -actin served as a loading control. **i** SA- β -gal staining analysis was performed as described for cells in **h**. Scale bar, 20 μ m. **j** Immunofluorescent staining of Mki67 in the cells from **i**. Scale bar, 5 μ m. The error bars show the s.d obtained from triplicate independent experiments. Two-tailed unpaired Student's *t*-tests were performed, ***p* < 0.01, ****p* < 0.001

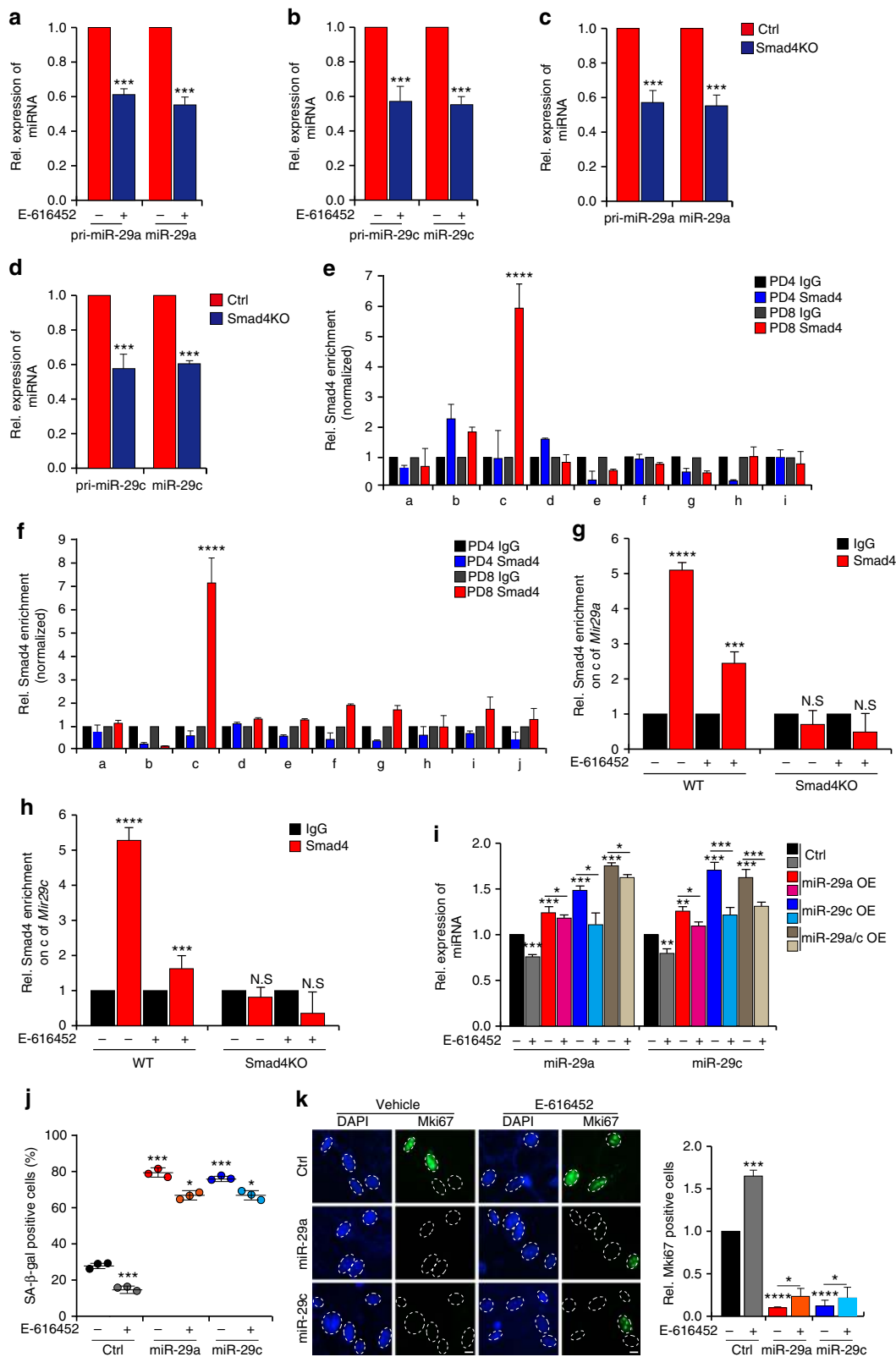
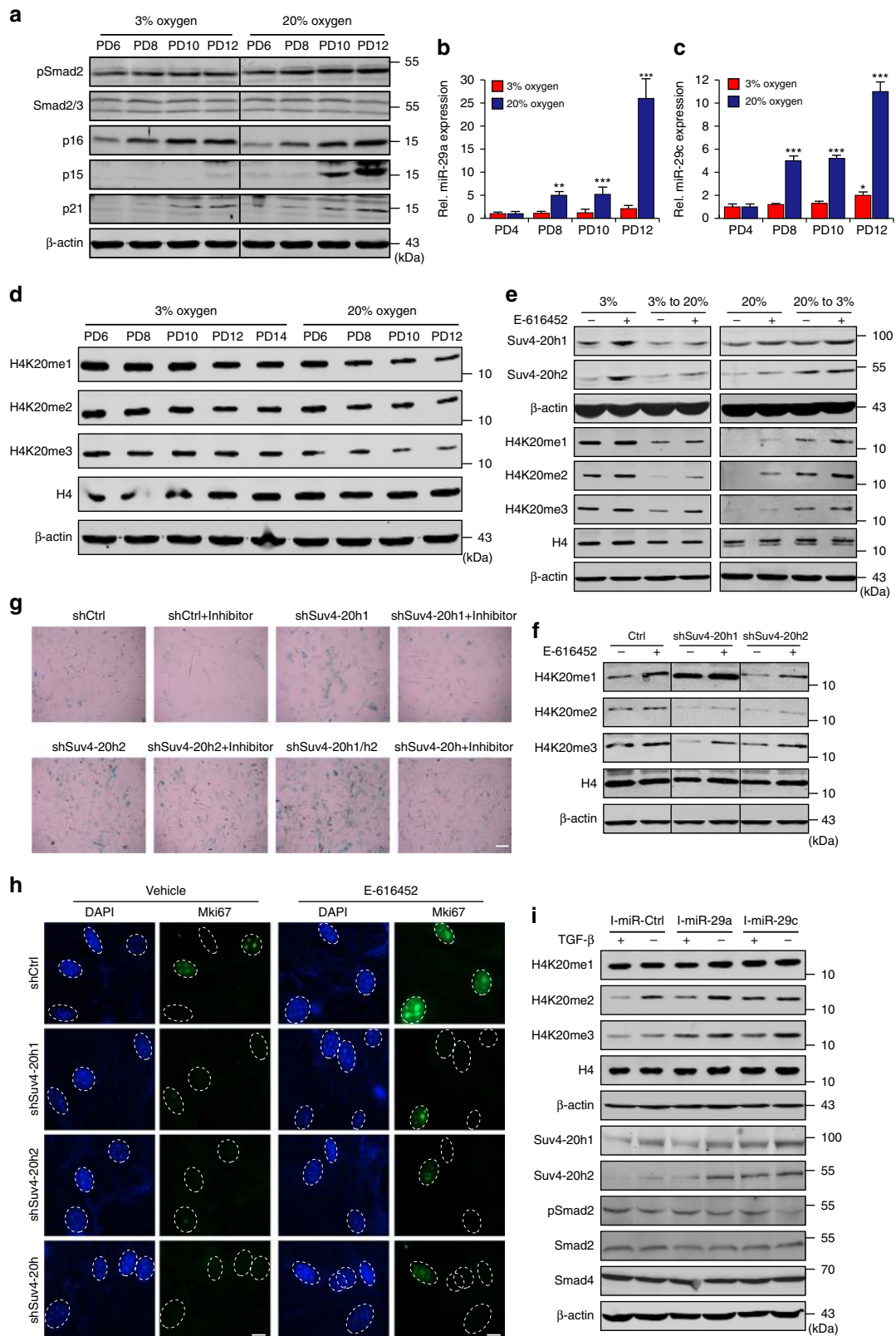


Fig. 3 TGF-β signaling regulates miR-29 expression in a Smad-dependent manner during MEFs senescence. **a-d** Quantitative real-time PCR for pri-miR-29 and miR-29 in MEFs incubated with E-616452 (**a, b**) or *Smad4* knockout (*Smad4*KO) MEFs (**c, d**). **e, f** Chromatin immunoprecipitation-qPCR (ChIP-qPCR) assays of *Smad4* from PD4 and PD8 MEFs. The x-axis represents the primer positions of the predicted promoters of *Mir29a* (**e**) and *Mir29c* (**f**). **g, h** *Smad4* enrichment on *Mir29a* (**g**) and *Mir29c* (**h**) was measured in inhibitor-treated MEFs and *Smad4*KO MEFs. **i** MEFs with lentivirus-mediated expression of miR-29 were incubated with E-616452. Real-time PCR was used to measure miR-29 expression. **j** Diagrams showing SA-β-gal staining of MEFs collected from **i**. **k** Immunofluorescent staining showing the Mki67 signals in MEFs with the same treatment as those shown in **i**. Scale bar, 5 μm. The error bars represent the s.d. obtained from triplicate independent experiments. Two-tailed unpaired Student's *t*-tests were performed, ***p* < 0.01, ****p* < 0.001

accelerates aging in vivo. We collected tissues samples (heart, liver, spleen, lung and kidney) from mice at different ages and found no significant change in the relative amount of H4K20m3 in the spleen or lung tissues as the age of the mice increased, although there was a slight increase in the relative amount of

H4K20m3 in the kidney (Supplementary Fig. 7a). However, the older mice exhibited accumulation of cardiac miR-29 (Fig. 6a) and steady reduction in the abundance of H4K20 methylation (Fig. 6b). In addition, fluctuation in the abundance of H4K20me3 was observed in the liver; H4K20me3 abundance increased



from 1 month of age to 6 months of age, after which it was decreased in mice aged 1 year and 2 years (Supplementary Fig. 7b). After the mice were fed with E-616452 to inhibit TGF- β signaling, decreased H4K20me3 abundance was observed in the livers of 1-year-old mice, but a substantial increase was observed in the livers of 2-year-old mice (Supplementary Fig. 7c). These results suggest that modulation of H4K20me3 by TGF- β signaling might be involved in cardiac aging, probably because the cardiovascular system consumes a relatively large amount of oxygen and therefore it is likely to be more susceptible than other tissues to hyperoxic stress. Indeed, inhibition of TGF- β signaling led to down-regulation of cardiac miR-29 (Fig. 6c), concomitant with restoration of H4K20me3 (Fig. 6d).

We applied echocardiographic imaging to analyze the left ventricular function of young (2-month-old, 2m) mice treated with DMSO or Suv4-20h inhibitor A-196 and old (1-year-old, 1y) mice fed with DMSO or T β RI inhibitor E-616452. In young mice, imaging analysis under B-mode, M-mode and pulsed wave Doppler-mode showed that A-196 treatment reduced the abundance of H4K20me3 (Supplementary Fig. 7d), weakened muscular movement of the left ventricle, decreased mitral flow and impaired systolic/diastolic function (Fig. 6e, f; Supplementary Fig. 7e and Supplementary Table 1), suggesting that H4K20me3 might be involved in protecting cardiac function. Treatment with E-616452 enhanced muscular movement of the left ventricle and partially rehabilitated mitral flow in old mice (Fig. 6e, f; Supplementary Fig. 7f and Supplementary Table 1), implying that inhibition of TGF- β signaling can contribute to preventing the age-associated declines in cardiac function. To validate the role of the TGF- β /miR-29 axis in regulating cardiac function, we isolated cardiomyocytes from adult mice aged 2 months (2m), 6 months (6m), and 1 year (1y) (Fig. 6g, h). The cardiomyocytes of the 1y adult mice showed increased SA- β -gal staining, activated TGF- β signaling, increased miR-29 accumulation and reduced abundance of H4K20me3 (Fig. 6i–l). Taken together, these results suggest that TGF- β /miR-29 signaling may contribute to age-associated cardiac dysfunction in vivo.

Discussion

Our results demonstrate that H4K20me3, serving as a responsive epigenetic target of canonical TGF- β signaling, is negatively regulated by miR-29 during the progression of senescence, followed by specific epigenetic alterations. Thus, our findings illustrate a sequential regulatory network of cellular senescence, in which external stimuli (e.g., atmospheric hyperoxia) trigger accelerated up-regulation of TGF- β signaling, and the subsequent initiation and progression of senescence are dependent on miR-29-modulated dysregulation of H4K20me3. Therefore, senescence is regulated on the epigenetic level downstream of TGF- β receptor activation (Fig. 6m).

miRNAs are highly conserved single-stranded, non-coding RNA molecules of 18–25 nucleotides in length, which are involved in post-transcriptionally governing expression of their targets in a myriad of physiological processes including

embryonic development⁵⁵, immune responses^{56,57}, cellular senescence and aging⁵⁸. In recent years, miRNAs have emerged as crucial regulators of age-related alterations in organ function⁵⁹, and the function of the cardiovascular system in particular^{42,43,60}. For example, age-induced expression of miR-34a and inhibition of its target PNUMS act as a key mechanism that regulates cardiac contractile function during aging and after acute myocardial infarction. In another study, miR-29 was found to be regulated by acute myocardial infarction (MI) in the region of the heart adjacent to the infarct, and TGF- β signaling decreased expression of miR-29 after MI⁴². Some researchers have reported that increased miR-29 expression is closely associated with cardiac aging in aged mice and killifish^{61,62}. These findings indicate that aging and other pathological contexts determine the regulatory response pattern of miR-29 downstream of TGF- β signaling. Here we found senescence- and aging-dependent miR-29 expression in fibroblasts and cardiomyocytes, and we established a potential link between miR-29 and TGF- β signaling. Therefore, it is reasonable to speculate that increased miR-29 expression might be a hallmark of cellular senescence and aging, and manipulation of the TGF- β /miR-29 pathway may provide opportunities for therapeutic modulation of aging and improvement of cardiac function.

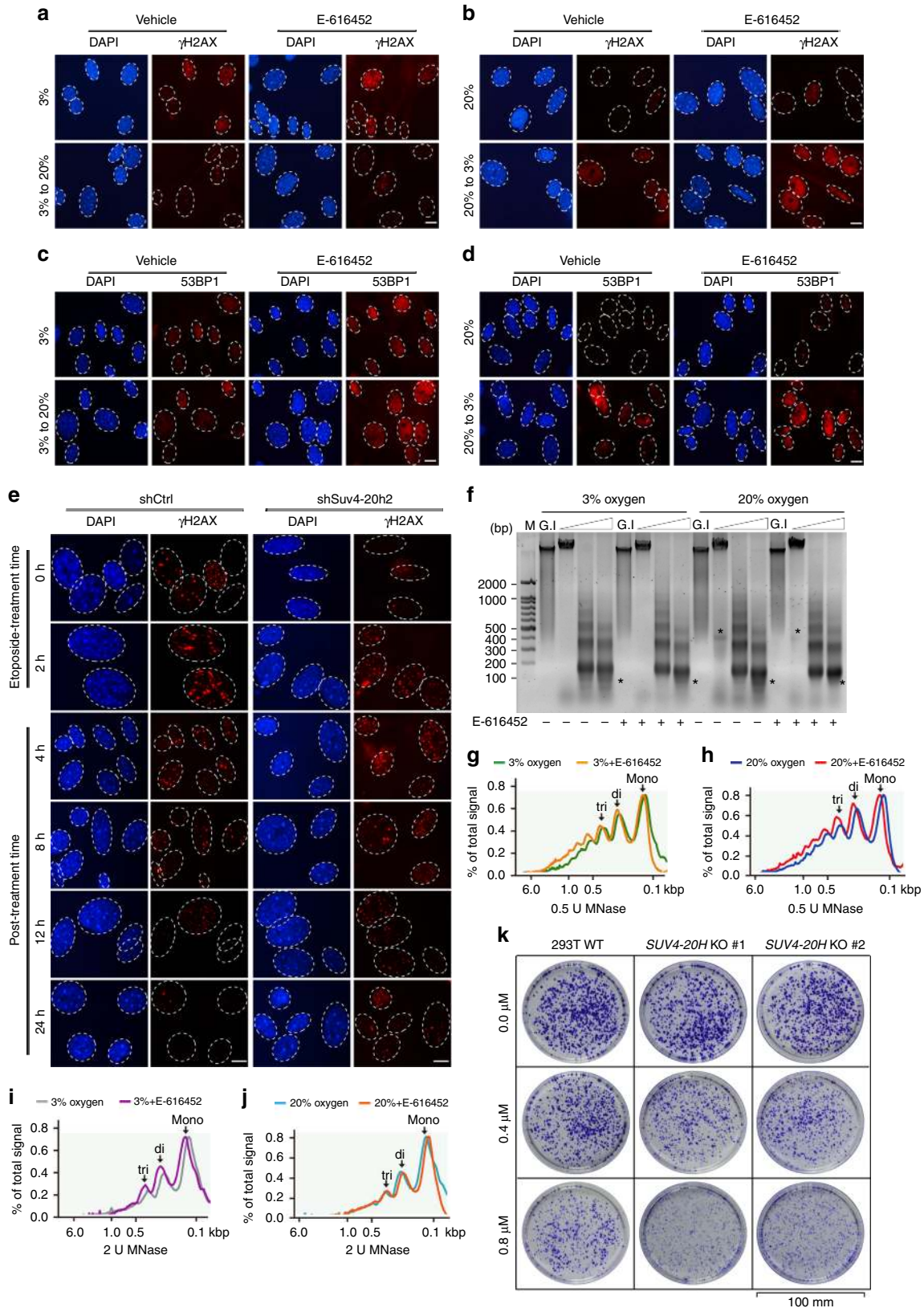
It is noteworthy that, in contrast to our findings in MEFs, the abundance of H4K20me3 was found to be increased in prematurely senescent HGPS (Hutchinson–Gilford Progeria Syndrome) cells⁶³, replicative and oncogene-induced senescent human diploid IMR90 fibroblasts⁶⁴, and *Zmpste24* deficiency-mediated early senescent MEFs in culture⁶⁵. Since TGF- β signaling is dynamically regulated in oncogene-induced and etoposide-induced senescence of IMR90 cells¹⁸, the seemingly paradoxical alterations of H4K20me3 abundance in models of senescence may be due to cell-type-specific and context-dependent TGF- β signaling. Indeed, H4K20me3 abundance was found to be increased in aged rat livers⁶⁶, while aged murine cardiomyocytes, human umbilical vein endothelial cells (HUVECs) and human embryonic fibroblasts (HEFs) exhibited senescent phenotypic alterations of H4K20me3 similar to that of MEFs (Supplementary Fig. 8a–d and Supplementary Fig. 9). In addition, abolition of TGF- β signaling inhibited miR-29 expression and restored H4K20me3 abundance in the heart, but not in the kidney, lung and spleen, which indicated that the cell and tissue contexts determine the specific response to TGF- β during senescence and aging. Therefore, we propose that a loss of H4K20me3 mediated by TGF- β /miR-29 contributes to senescence and aging in a cellular-context and tissue-specific manner.

We also noted that increased H4K20me3 abundance was accompanied by down-regulated TGF- β signaling in *Zmpste24*-deficient MEFs (Supplementary Fig. 10a–j). Considering that disruption of the nuclear periphery structure perturbs signal transduction⁶⁷, depletion of *Zmpste24* may negatively affect TGF- β -miR-29 signaling. Indeed, although the abundance of H4K20me3 was increased in *Zmpste24*-knockout cells in comparison with the same passage of wild-type cells, a global loss of

Fig. 4 Regulation of senescence by TGF- β signaling is dependent on miR-29-induced inhibition of H4K20me3. **a** Western blot for the indicated proteins in MEFs grown in 3% oxygen or 20% oxygen. β -actin served as a loading control. **b, c** RT-qPCR analysis of miR-29 expression in the cells from **a**. **d** Western blot to assess total H4K20 methylation in serially passaged MEFs grown in 3% oxygen or 20% oxygen. β -actin served as a loading control. **e** MEFs grown in 3% oxygen and transferred to 20% oxygen (left) or MEFs grown in 20% oxygen and transferred to 3% oxygen (right) were treated with or without inhibitors. Protein changes were tested by western blot. H4 and β -actin served as loading controls. **f** Western blots showing altered H4K20 methylation in MEFs incubated with or without inhibitors upon knockdown of shCtrl, Suv4-20h1, Suv4-20h2 or both. **g** SA- β -gal staining showing alterations in the SA- β -gal signal in the cells from **f**. Scale bar, 20 μ m. One-way ANOVA with Dunnett's multiple comparison test analysis was performed. **h** Immunofluorescent staining showing the Mki67 signal in MEFs exposed to the same treatment as those shown in **f**. Scale bar, 5 μ m. **i** Western blot for analyzing the indicated proteins in MEFs subjected to inhibition of miR-29 expression followed by TGF- β treatment. H4 and β -actin served as loading controls. The error bars represent the s.d. obtained from triplicate independent experiments. Two-tailed unpaired Student's *t*-tests were performed, ***p* < 0.01, ****p* < 0.001

H4K20me3 occurred during serial passages of *Zmpste24*-knock-out cells (Supplementary Fig. 10k), and inhibition of TGF- β signaling led to elevated H4K20 methylation (Supplementary Fig. 10l, m) and decreased miR-29 expression (Supplementary Fig. 10n, o) in

the late passages of wild-type and *Zmpste24*-depleted cells. These observations suggest that depletion of *Zmpste24* blocks TGF- β -miR-29 signaling, which in turn results in elevated H4K20me3. The findings described above suggest that H4K20me3 is



distinctively regulated in various senescent cell types and aging scenarios, which should be further explored in future studies.

Finally, we showed that E-616452, an inhibitor of TGF- β signaling, is capable of restoring the global H4K20me3 level in vivo and in vitro to establish a more “youthful” H4K20me3 signature. E-616452 is an essential compound in a cocktail used to chemically induce pluripotent stem cells⁶⁸. Given that cellular senescence is not a limit to reprogramming^{69,70}, and small molecule compounds can completely replace exogenous transgenes to generate pluripotent epigenetic and gene transcriptional profiles following somatic cell reprogramming, it appears possible to delay senescence or aging by targeting transcriptional networks and epigenetic features associated with cellular senescence using certain combinations of small-molecule compounds.

Methods

Generation of primary cells and cell culture. Primary mouse embryonic fibroblasts (MEFs) isolated from 12.5 to 14-day-old embryos of C57BL/6 mice, human embryonic fibroblasts (HEFs) isolated from 2- to 3-month-old human female embryos, and HEK293T from American Type Culture Collection (ATCC) were cultured in DEME (GIBCO, Grand Island, NY, USA), supplemented with 10% fetal bovine serum (FBS, GIBCO, Grand Island, NY, USA) and 1% Penicillin/Streptomycin (GIBCO, Grand Island, NY, USA), and incubated at 37 °C in a humidified incubator with 5% CO₂. HEFs were obtained with informed written consent and approval by the Clinical Research Ethics Committee of China-Japan Friendship Hospital (No. 2009-50). The whole procedure was conducted according to the principles of the Declaration of Helsinki. The culture medium was MEM supplemented with 10% FBS (GIBCO), and the culture dish was gelatin-coated before inoculation of primary human umbilical vascular endothelial cells (HUVECs) purchased from ALLCELLS Co. Ltd., Shanghai, China. Cells were tested for mycoplasma contamination according to the manufacturer's instructions (Mycobio Mycoplasma Detector, D101-01/02).

To develop replicative senescence, confluent MEFs, HEFs, and HUVECs were evenly transferred into new dishes, after which the cells were cultured until confluence to generate one population doubling (PD). Cells were maintained in a 100-mm dish. In this study, confluence was defined as a nearly confluent culture condition without contact inhibition. The number (n) of PDs was calculated using the equation $n = \log_2(N_e/N_s)$, where N_e and N_s are the numbers of cells at the end of cell culture and those seeded at the start of one passage, respectively. The numbers of population doublings (PDs, times), doubling time (DT, days), and total culturing period were monitored once every three days until the cells completely stopped proliferating.

To isolate cardiomyocytes from adult mice, myocytes were separated in a high potassium buffer from the isolated heart tissue samples by modified Langendorff perfusion with type II collagenase. The hearts were removed from the anesthetized mice and subjected to cannulation, perfusion and digestion. Calcium was reintroduced into the dissociated cardiomyocytes, which were used in the following experiments.

Senescence-associated β -galactosidase (SA- β -gal) staining. SA- β -gal activity, as a classic biomarker of senescent cells, was monitored for all MEFs growth stages of as described previously. The culture medium was removed from 6-well plates, after which the cells were washed once with 1 mL of 1 \times PBS and fixed with 0.5 mL of fixative solution for 10–15 min at room temperature. While the cells were in the fixative solution, the staining solution mixture (staining solution, staining supplement and 20 mg/mL X-gal in DMSO) was prepared according to the manufacturer's instructions (Sigma, CS0030, USA). The cells were washed twice with 1 mL of 1 \times PBS and incubated overnight with the staining mixture at 37 °C. The cells were observed under an inverted microscope with 10 \times 10 magnification (Leica DMI 6000B, Leica, Germany). The SA- β -gal signals were analyzed using Image J software (NIH).

Real time and quantitative PCR (RT-qPCR). Cells were harvested at 80% confluence. Total RNA was isolated with TRIzol Reagent (Invitrogen, 15596018, USA)

according to the provided instructions. For RT-qPCR analysis, total RNA was reverse-transcribed into cDNA using random hexamer primers, and cDNA generated from mRNA, pri-miRNA and pre-miRNA levels was measured by qPCR (LightCycler, Roche, Swiss) with specific primers, after which the results were normalized using *Gapdh*. For mature miRNA, miRNA was reverse-transcribed according to the manufacturer's instructions (Tiangen, KR211-02, China) and measured by qPCR with specific forward primers (see Supplementary Table 2) and commercially available reverse primers.

Western blot. Total protein samples were resolved in 1% SDS, subjected to SDS-PAGE, transferred to nitrocellulose membranes and incubated overnight with primary antibodies of interest at 4 °C. The primary antibodies were anti-H3K4me3 (1:1000, Millipore, 04-745), anti-H3K9me1 (1:1000, Abcam, ab9045), anti-H3K9me2 (1:1000, Abcam, ab1220), anti-H3K9me3 (1:1000, Abcam, ab8898), anti-H3K9Ac (1:1000, Millipore, 07-352), anti-H3K27me3 (1:1000, Millipore, 07-449), anti-H3K36me2 (1:1000, Abcam, ab9049), anti-H3K36me3 (1:1000, Abcam, ab9050), anti-H4K16Ac (1:1000, Millipore, 07-329), anti-H4K20me1 (1:1000, Abcam, ab9051), anti-H4K20me2 (1:1000, Abcam, ab9052), anti-H4K20me3 (1:1000, Abcam, ab9053), anti-H3 (1:1000, Abcam, ab1791), anti-H4 (1:1000, Abcam, ab10158), anti-Suv4-20h1 (1:500, Abcam, ab118659), anti-Suv4-20h2 (1:500, Abcam, ab91224), anti- β -actin (1:2000, Santa Cruz, sc-47778), anti-p16 (1:1000, Santa Cruz, sc-1207), anti-p15 (1:500, Santa Cruz, sc-612), anti-p21 (1:500, Abcam, ab109199), anti-pSmad2 (1:1000, CST, #3101), anti-Smad2/3 (1:1000, CST, #3102), anti-Smad4 (1:1000, Abcam, ab40759), anti- γ H2AX (1:1000, CST, #9718P), anti-Gapdh (1:2000, ZSGB-BIO, TA-08) and anti- α -tubulin (1:2000, Sigma, T9026). The blots were then washed three times in PBST (1 \times PBS and 0.1% Tween-20) and incubated with diluted secondary antibodies IRDye800CW Goat/Donkey anti-Mouse/Rabbit (1:10000, LI-COR, 926-32210) for 2 h at room temperature. Finally, the blots were washed three times with PBST and visualized using an Odyssey Infrared Imaging System (Odyssey, LI-COR).

Uncropped western blots can be found in Supplementary Figs. 11 and 12.

Immunofluorescent microscopy. Cells were plated on clean cover slides in 100-mm culture dishes. When the cells reached 70–80% confluence, the cells on the slides were washed twice with ice-cold 1 \times PBS and fixed with 4% paraformaldehyde for 10 min at room temperature. The cells were washed three times with 1 \times PBS at room temperature, after which the cover slide was transferred to a humid dish. Next, 1% BSA was utilized to block the cells at room temperature for 30 min. The cells were washed three times with 1 \times PBS and incubated overnight at 4 °C with 150 μ L of primary antibodies diluted in PBST. The primary antibodies were anti-Ki67 (1:400, Abcam, ab15580), anti- γ H2AX (1:300, CST, #9718P), and anti-53BP1 (1:200, Abcam, ab36823). The cells were washed 4 times with PBST and incubated at room temperature for 2 h with 150 μ L of secondary antibodies (1:500, Alexa Fluor 488 Donkey Anti-Mouse or Alexa Fluor 594 Donkey Anti-Rabbit, Life Technologies) diluted in PBST. The cells were washed three times with PBST and incubated with 1 ng/ μ L of DAPI at room temperature for 3 min. The cells were washed 3 times with 1 \times PBS, followed by a wash with ddH₂O, after which the cover slide was sealed with 10 μ L of Fluoromount-G. After 1 h, images of the cells were captured under a fluorescent microscope. The immunofluorescent signals were examined using Image J software (NIH).

Luciferase reporter assay. For the luciferase assays of the miRNA targets, constructs were generated by inserting the full-length 3' UTRs of mouse *Suv4-20h1* and *Suv4-20h2* into the pmirGLO vector (Promega, E1330) with specific primers. In total 50 nM of mimics and inhibitors of miRNAs were co-transfected with the constructs into HEK293T cells, respectively, using Lipofectamine 2000 (Invitrogen, 11668-027). Mimics and inhibitors of miR-29a and miR-29c were synthesized in RiboBio, China. In addition, the putative miR-29a and miR-29c seed sequence binding site (5'-TGTTGCT-3') in the 3' UTR of *Suv4-20h1* was mutated to 5'-CGTACC-3', meanwhile the two putative miR-29a and miR-29c seed sequence binding sites (5'-GTGCTAT-3' and 5'-TGTTGCT-3') in 3' UTRs of *Suv4-20h2* were mutated to 5'-CTCCAAT-3' (Mut-1), 5'-AGTCCA-3' (Mut-2) or both of these sequences. To test promoter activity utilizing luciferase assays, the predicted promoter regions of *Id1*, *p21*, *Mir29a* and

Fig. 5 H4K20me3 contributes to DNA damage repair and genome maintenance. **a–d** MEFs cultured under the indicated conditions and treated with or without inhibitors were collected for immunofluorescent staining of γ H2AX (**a, b**) or 53BP1 (**c, d**). Scale bar, 5 μ m. **e** Etoposide-treated control (shCtrl) or *Suv4-20h2* knockdown (shSuv4-20h2) cells were subjected to γ H2AX staining according to the indicated time course. Scale bar, 5 μ m. **f–j** Nuclei from cells grown in 3% oxygen or 20% oxygen and treated with or without E-616452, were incubated with 0, 0.5 or 2 U of MNase for 5 min followed by DNA extraction, agarose gel electrophoresis and ethidium bromide staining. The asterisks indicate prominent fragment changes (**f**). The band densities were quantified using Image J software and illustrated as percentage of the signal subtracted background of the entire line from top to the bottom. Calibrated kilobase pair (kbp) sizes are indicated (**g–j**). **k** Wild-type HEK293T (293T WT) and *SUV4-20H* knockout cells (*SUV4-20H* KO #1 and *SUV4-20H* KO #2) were treated with the indicated concentration of etoposide, followed by crystal violet staining. Scale bar, 100 μ m

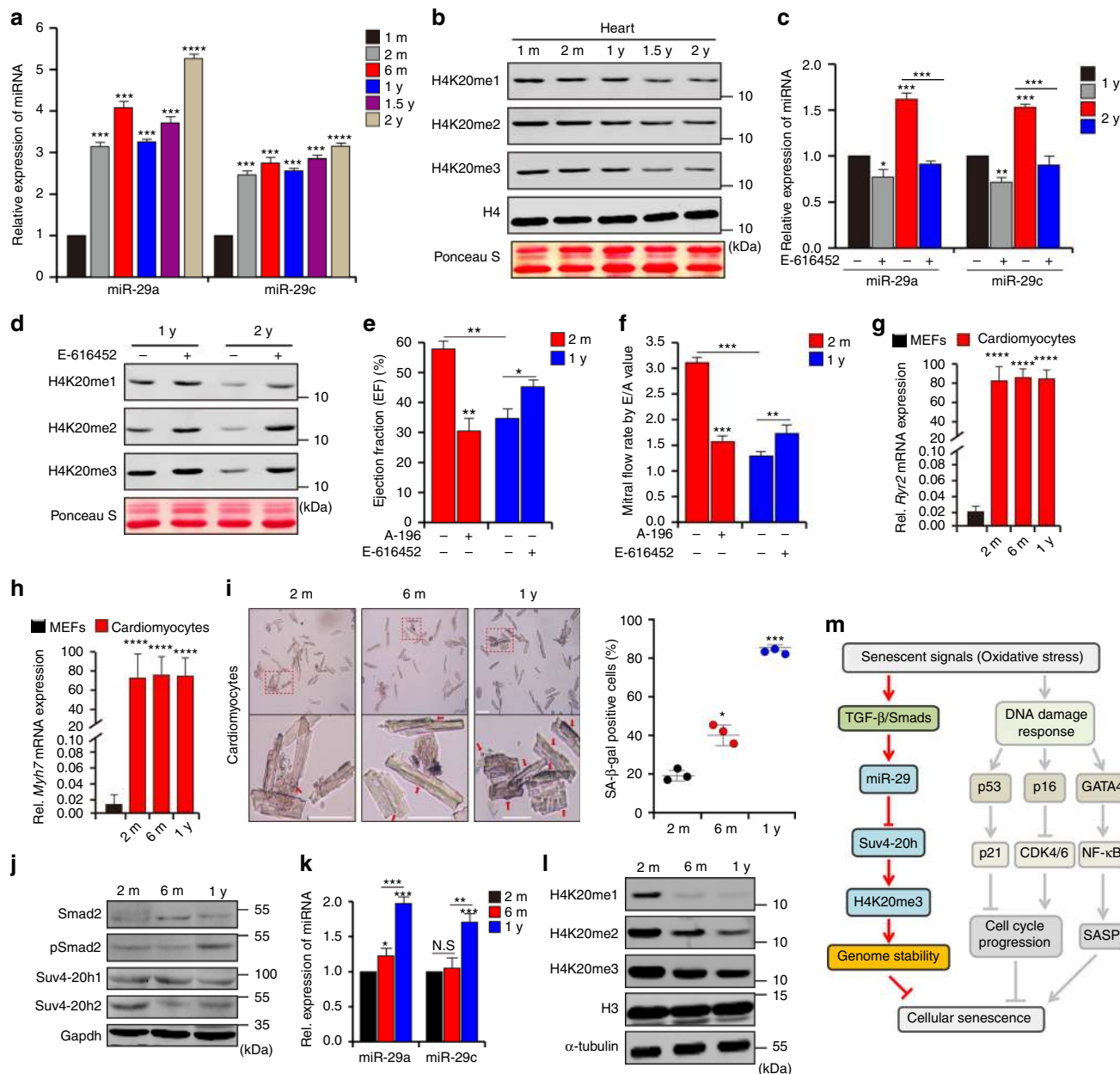


Fig. 6 TGF- β /miR-29/H4K20me3 is involved in aging-associated cardiac dysfunction. **a** RT-qPCR to measure miR-29 expression, normalized to U6, in murine hearts ($n = 4$ per age) of the indicated ages (1-month-old, 1 m; 2-month-old, 2 m; 1-year-old, 1 y; 1.5-year-old, 1.5 y; 2-year-old, 2 y). **b** Western blot for H4K20 methylation in hearts of the indicated ages. **c** RT-qPCR to examine miR-29 expression in hearts of 1 y and 2 y mice, fed with DMSO or E-616452. The error bars represent the s.d. obtained from triplicate independent experiments. **d** Western blot for H4K20 methylation in hearts from **c**. **e**, **f** Mice (2 m) fed with DMSO ($n = 4$) or A-196 ($n = 4$) and mice (1 y) treated with DMSO ($n = 8$) or E-616452 ($n = 8$) were subjected to cardiac function analysis using an echocardiographic imaging system (VisualSonics Vevo 2100, USA). EF (**e**) represents the ejection fraction of left ventricular flow, whereas E/A (**f**), the peak early filling (E-wave)/late diastolic filling (A-wave), represents the mitral flow rate. Representative images are shown in Supplementary Fig. 7e, f. The error bars represent the s.d. of the mean values. **g**, **h** RT-qPCR analysis of *Ryr2* (**g**) and *Myh7* (**h**) expression in cardiomyocytes isolated from mice of the indicated ages. **i** SA- β -gal staining of cardiomyocytes from mice as in **g**. The lower panel shows the magnified cells enclosed by red rectangular boxes in the images in the upper panel. Scale bar = 20 μ m. The plot shows the proportion of SA- β -gal-stained cells among the different age groups. **j** Western blot for the indicated proteins in cells from **i**. **k** RT-qPCR for miR-29 expression in isolated cells from **i**. **l** Western blot for H4K20 methylations in cells from **f**. **m** Mechanisms proposed in this study. When cells undergo senescence-inducing stimuli, such as oxidative stress, TGF- β signaling is activated and serves as the signal transducer that promotes acute accumulation of miR-29, which in turn results in suppression of Suv4-20h and reduction in H4K20me3 abundance, leading to defective DNA damage repair and impaired maintenance of genome stability, and thus accelerating cellular senescence. Gapdh, H3 and α -tubulin were loading controls. Two-tailed unpaired Student's *t*-tests, * $p < 0.05$, ** $p < 0.01$, *** $p < 0.001$

Mir29c obtained from UCSC and NCBI were cloned into pGL3 (Promega) upstream of the luciferase gene. The empty or Smad4 overexpression vectors and recombinant pGL3 were co-transfected into HEK293T cells, and luciferase activity was monitored 24 h later. Luciferase activity was tested using the Dual-Glo Luciferase Assay Kit (Promega, E2920).

Chromatin immunoprecipitation. Approximately 1.2×10^6 MEFs were cross-linked with 1% paraformaldehyde for 10 min at room temperature. After quenching the paraformaldehyde reaction with 0.125 M glycine for 5 min, cells were harvested, lysed with nuclear lysis buffer (50 mM Tris-Cl, 10 mM EDTA, 1% SDS and protease inhibitors) on ice and sonicated with Bioruptor (Diagenode,

Belgium) for the chromatin immunoprecipitation assays. Fragmented chromatin (25 µg) was subjected to immunoprecipitation with 4 µg of anti-Smad4 antibody (Abcam, ab40759) or anti-Rabbit IgG (Abcam, ab171870). The immunoprecipitated DNA was quantified by RT-qPCR. The ratio of DNA in the immunoprecipitates was calculated versus 10% input chromatin. The primer sequences used in this analysis are included in the Supplementary Table 2.

Lentiviral production and viral transduction. To produce the lentiviruses of interest, HEK293T cells were transiently co-transfected with pLKO.1-shRNA encoding shRNAs targeting Suv4-20h1, Suv4-20h2 or Smad4 (TRC library, Sigma), as well as assistant vectors psPAX and pMD2.G. The culture medium was replaced with DMEM supplemented with 30% FBS 18 h later, and viral supernatants were collected 24 h later. Cells were infected with the packaged viruses with 5 µg/mL polybrene (M&C Gene Technology, MC032, China). 36–48 h after infection, cells were selected in 3 µg/mL of puromycin (M&C Gene Technology, MA009, China) for 24–36 h, after which they were plated into different dishes. Cells were then continuously selected in 1 µg/mL of puromycin for 4–5 days until no dead cells were found in the dishes.

Nucleosomal DNA preparation. MEFs were collected in 1× PBS and resuspended in lysis buffer (15 mM Hepes, pH 7.4, 85 mM KCl and 0.5% NP-40) in the presence of a protease inhibitors cocktail (Roche) and PMSF, after which the nuclei were pelleted. The nuclei pellets were washed and resuspended in MNase digestion buffer (320 mM sucrose, 50 mM Tris-HCl, pH 7.5, 4 mM MgCl₂, 1 mM CaCl₂, 0.1 mM PMSF). To generate nucleosomal material, digestions were conducted by adding 0, 0.5 and 2 U of MNase per 0.1 mL of MNase digestion buffer. The reaction was incubated for 2 min at 37 °C and stopped by adding EGTA to a final concentration of 20 mM. The digested material was treated with RNase for 30 min at 37 °C, followed by Proteinase K treatment and two pheno-chloroform extractions. DNA was isolated from the extracted supernatant used to by adding with 3 M NaAc (pH 5.2) to a final concentration of 0.3 M Na⁺, 40 µg of glycogen and two-fold volumes of absolute ethanol. The precipitated DNA was analyzed by agarose gel electrophoresis and stained with ethidium bromide.

Clonogenic cell survival assay. Wild-type and *SUV4-20H*-knockout cells (500 cells each) were plated separately in 100-mm culture dishes in triplicate and treated with etoposide at different final concentrations for 6 h, after which the medium was replaced with fresh medium without etoposide. Twelve days later, the cells were washed with 1×PBS, fixed with 4% formaldehyde for 15 min and stained with crystal violet (0.1% wt/vol) for 30 min. The number of colonies per dish was counted.

Animal models. All animal experiments were approved by the Institutional Animal Care and Use Committee of Peking University. The mice used in this study were examined by the investigator in a double-blinded manner. When performing the echocardiographic imaging, the investigator lacked information regarding the treatment and was aware of only the strain and sex of the test mouse. Mice used in this study were not randomly chosen, and female and male mice were included.

Statistical analysis. Approximately 100–300 cells were counted per sample, and three independent experiments were carried out. The data were analyzed by either a two-tailed unpaired Student's *t*-test or one-way ANOVA with Dunnett's multiple comparison test analysis (GraphPad Prism software, version 5.01). The results are expressed as mean ± s.d. Probability values (*p*) <0.05 were considered to be statistically significant.

Data availability. All data supporting the findings in this study are available from the corresponding author upon reasonable request.

Received: 26 June 2017 Accepted: 22 May 2018

Published online: 02 July 2018

References

- Dimri, G. P. et al. A biomarker that identifies senescent human cells in culture and in aging skin in vivo. *Proc. Natl Acad. Sci. USA* **92**, 9363–9367 (1995).
- Coppé, J.-P. et al. Senescence-associated secretory phenotypes reveal cell-nonautonomous functions of oncogenic RAS and the p53 tumor suppressor. *PLoS Biol.* **6**, e301 (2008).
- Rodier, F. & Campisi, J. Four faces of cellular senescence. *J. Cell Biol.* **192**, 547–556 (2011).
- Burd, C. E. et al. Monitoring tumorigenesis and senescence in vivo with a p16 (INK4a)-luciferase model. *Cell* **152**, 340–351 (2013).
- Serrano, M., Lin, A. W., McCurrach, M. E., Beach, D. & Lowe, S. W. Oncogenic ras provokes premature cell senescence associated with accumulation of p53 and p16 INK4a. *Cell* **88**, 593–602 (1997).
- Michaloglou, C. et al. BRAFE600-associated senescence-like cell cycle arrest of human naevi. *Nature* **436**, 720–724 (2005).
- Kang, C. et al. The DNA damage response induces inflammation and senescence by inhibiting autophagy of GATA4. *Science* **349**, aaa5612 (2015).
- Childs, B. G., Durik, M., Baker, D. J. & van Deursen, J. M. Cellular senescence in aging and age-related disease: from mechanisms to therapy. *Nat. Med.* **21**, 1424–1435 (2015).
- Baker, D. J. et al. Naturally occurring p16Ink4a-positive cells shorten healthy lifespan. *Nature* **530**, 184–189 (2016).
- Storer, M. et al. Senescence is a developmental mechanism that contributes to embryonic growth and patterning. *Cell* **155**, 1119–1130 (2013).
- Munoz-Espin, D. & Serrano, M. Cellular senescence: from physiology to pathology. *Nat. Rev. Mol. Cell Biol.* **15**, 482–496 (2014).
- He, S. & Sharpless, N. E. Senescence in health and disease. *Cell* **169**, 1000–1011 (2017).
- Munoz-Espin, D. et al. Programmed cell senescence during mammalian embryonic development. *Cell* **155**, 1104–1118 (2013).
- Derynck, R., Akhurst, R. J. & Balmain, A. TGF-β signaling in tumor suppression and cancer progression. *Nat. Genet.* **29**, 117–129 (2001).
- Jang, C. W. et al. TGF-beta induces apoptosis through Smad-mediated expression of DAP-kinase. *Nat. Cell Biol.* **4**, 51–58 (2002).
- Akhurst, R. J. & Hata, A. Targeting the TGF beta signalling pathway in disease. *Nat. Rev. Drug Discov.* **11**, 790–811 (2012).
- Massagué, J. How cells read TGF-β signals. *Nat. Rev. Mol. Cell Biol.* **1**, 169–178 (2000).
- Hoare, M. et al. NOTCH1 mediates a switch between two distinct secretomes during senescence. *Nat. Cell Biol.* **18**, 979–992 (2016).
- Hannum, G. et al. Genome-wide methylation profiles reveal quantitative views of human aging rates. *Mol. Cell* **49**, 359–367 (2013).
- Horvath, S. DNA methylation age of human tissues and cell types. *Genome Biol.* **14**, 3156 (2013).
- Zhang, W. et al. A Werner syndrome stem cell model unveils heterochromatin alterations as a driver of human aging. *Science* **348**, 1160–1163 (2015).
- Kawahara, T. L. et al. SIRT6 links histone H3 lysine 9 deacetylation to NF-κB-dependent gene expression and organismal life span. *Cell* **136**, 62–74 (2009).
- Sen, P. et al. H3K36 methylation promotes longevity by enhancing transcriptional fidelity. *Genes Dev.* **29**, 1362–1376 (2015).
- Chandra, T. & Kirschner, K. Chromosome organisation during ageing and senescence. *Curr. Opin. Cell Biol.* **40**, 161–167 (2016).
- Criscione, S. W. et al. Reorganization of chromosome architecture in replicative cellular senescence. *Sci. Adv.* **2**, e1500882 (2016).
- Abdelmohsen, K. et al. Senescence-associated lncRNAs: senescence-associated long noncoding RNAs. *Aging Cell* **12**, 890–900 (2013).
- Montes, M. et al. The lncRNA MIR31HG regulates p16(INK4A) expression to modulate senescence. *Nat. Commun.* **6**, 6967 (2015).
- Benayoun, B. A. P. & Elizabeth, A. Brunet Anne Epigenetic regulation of ageing: linking environmental inputs to genomic stability. *Nat. Rev. Mol. Cell Biol.* **16**, 593–610 (2015).
- di Val Cervo, P. R. et al. p63–microRNA feedback in keratinocyte senescence. *Proc. Natl Acad. Sci. USA* **109**, 1133–1138 (2012).
- Benhamed, M., Herbig, U., Ye, T., Dejean, A. & Bischof, O. Senescence is an endogenous trigger for microRNA-directed transcriptional gene silencing in human cells. *Nat. Cell Biol.* **14**, 266–275 (2012).
- He, J., Kallin, E. M., Tsukada, Y. & Zhang, Y. The H3K36 demethylase Jhdmlb/Kdm2b regulates cell proliferation and senescence through p15 (INK4b). *Nat. Struct. Mol. Biol.* **15**, 1169–1175 (2008).
- Tanaka, H. et al. The SETD8/PR-Set7 methyltransferase functions as a barrier to prevent senescence-associated metabolic remodeling. *Cell Rep.* **18**, 2148–2161 (2017).
- Greer, E. L. et al. Members of the H3K4 trimethylation complex regulate lifespan in a germline-dependent manner in *C. elegans*. *Nature* **466**, 383–387 (2010).
- Narita, M. et al. Rb-mediated heterochromatin formation and silencing of E2F target genes during cellular senescence. *Cell* **113**, 703–716 (2003).
- Merkwirth, C. et al. Two conserved histone demethylases regulate mitochondrial stress-induced longevity. *Cell* **165**, 1209–1223 (2016).
- Bromberg, K. D. et al. The SUV4-20 inhibitor A-196 verifies a role for epigenetics in genomic integrity. *Nat. Chem. Biol.* **13**, 317–324 (2017).
- Schotta, G. et al. A chromatin-wide transition to H4K20 monomethylation impairs genome integrity and programmed DNA rearrangements in the mouse. *Genes Dev.* **22**, 2048–2061 (2008).

38. Jonas, S. & Izaurralde, E. Towards a molecular understanding of microRNA-mediated gene silencing. *Nat. Rev. Genet.* **16**, 421–433 (2015).
39. Bartel, D. P. MicroRNAs: genomics, biogenesis, mechanism, and function. *Cell* **116**, 281–297 (2004).
40. Griffiths-Jones, S., Saini, H. K., van Dongen, S. & Enright, A. J. miRBase: tools for microRNA genomics. *Nucleic Acids Res.* **36**, D154–D158 (2008).
41. Agarwal, V., Bell, G. W., Nam, J.-W. & Bartel, D. P. Predicting effective microRNA target sites in mammalian mRNAs. *eLife* **4**, e05005 (2015).
42. van Rooij, E. et al. Dysregulation of microRNAs after myocardial infarction reveals a role of miR-29 in cardiac fibrosis. *Proc. Natl Acad. Sci. USA* **105**, 13027–13032 (2008).
43. Olson, E. N. MicroRNAs as therapeutic targets and biomarkers of cardiovascular disease. *Sci. Transl. Med.* **6**, 239ps233–239ps233 (2014).
44. Ru, P. et al. Feedback loop regulation of SCAP/SREBP-1 by miR-29 modulates EGFR signaling-driven glioblastoma growth. *Cell Rep.* **16**, 1527–1535 (2016).
45. Wang, J., Wang, Y., Ma, Y., Lan, Y. & Yang, X. Transforming growth factor β -regulated microRNA-29a promotes angiogenesis through targeting the phosphatase and tensin homolog in endothelium. *J. Biol. Chem.* **288**, 10418–10426 (2013).
46. Davis, B. N., Hilyard, A. C., Lagna, G. & Hata, A. SMAD proteins control DROSHA-mediated microRNA maturation. *Nature* **454**, 56–61 (2008).
47. Roy, S. et al. Fra-2 mediates oxygen-sensitive induction of transforming growth factor beta in cardiac fibroblasts. *Cardiovasc. Res.* **87**, 647–655 (2010).
48. Parrinello, S. et al. Oxygen sensitivity severely limits the replicative lifespan of murine fibroblasts. *Nat. Cell Biol.* **5**, 741–747 (2003).
49. Pei, H. et al. MMSSET regulates histone H4K20 methylation and 53BP1 accumulation at DNA damage sites. *Nature* **470**, 124–128 (2011).
50. Jorgensen, S., Schotta, G. & Sorensen, C. S. Histone H4 lysine 20 methylation: key player in epigenetic regulation of genomic integrity. *Nucleic Acids Res.* **41**, 2797–2806 (2013).
51. Tuzon, C. T. et al. Concerted activities of distinct H4K20 methyltransferases at DNA double-strand breaks regulate 53BP1 nucleation and NHEJ-directed repair. *Cell Rep.* **8**, 430–438 (2014).
52. Collado, M., Blasco, M. A. & Serrano, M. Cellular senescence in cancer and aging. *Cell* **130**, 223–233 (2007).
53. Campisi, J. Aging, cellular Senescence, and cancer. *Annu. Rev. Physiol.* **75**, 685–705 (2013).
54. Lopez-Otin, C., Blasco, M. A., Partridge, L., Serrano, M. & Kroemer, G. The hallmarks of aging. *Cell* **153**, 1194–1217 (2013).
55. Wienholds, E. et al. MicroRNA expression in zebrafish embryonic development. *Science* **309**, 310–311 (2005).
56. Tsitsiou, E. & Lindsay, M. A. microRNAs and the immune response. *Curr. Opin. Pharmacol.* **9**, 514–520 (2009).
57. Ma, F. et al. The microRNA miR-29 controls innate and adaptive immune responses to intracellular bacterial infection by targeting interferon-gamma. *Nat. Immunol.* **12**, 861–869 (2011).
58. Kaikkonen, M. U., Lam, M. T. & Glass, C. K. Non-coding RNAs as regulators of gene expression and epigenetics. *Cardiovasc. Res.* **90**, 430–440 (2011).
59. Dimmeler, S. & Nicotera, P. MicroRNAs in age-related diseases. *EMBO Mol. Med.* **5**, 180–190 (2013).
60. Small, E. M. & Olson, E. N. Pervasive roles of microRNAs in cardiovascular biology. *Nature* **469**, 336–342 (2011).
61. Heid, J. et al. Age-dependent increase of oxidative stress regulates microRNA-29 family preserving cardiac health. *Sci. Rep.* **7**, 16839 (2017).
62. Boon, R. A. et al. MicroRNA-34a regulates cardiac ageing and function. *Nature* **495**, 107–110 (2013).
63. Shumaker, D. K. et al. Mutant nuclear lamin A leads to progressive alterations of epigenetic control in premature aging. *Proc. Natl Acad. Sci. USA* **103**, 8703–8708 (2006).
64. Nelson, D. M. et al. Mapping H4K20me3 onto the chromatin landscape of senescent cells indicates a function in control of cell senescence and tumor suppression through preservation of genetic and epigenetic stability. *Genome Biol.* **17**, 158 (2016).
65. Liu, B. et al. Depleting the methyltransferase Suv39h1 improves DNA repair and extends lifespan in a progeria mouse model. *Nat. Commun.* **4**, 1868 (2013).
66. Sarg, B., Koutzamani, E., Helliger, W., Rundquist, I. & Lindner, H. H. Postsynthetic trimethylation of histone H4 at lysine 20 in mammalian tissues is associated with aging. *J. Biol. Chem.* **277**, 39195–39201 (2002).
67. Andres, V. & Gonzalez, J. M. Role of A-type lamins in signaling, transcription, and chromatin organization. *J. Cell Biol.* **187**, 945–957 (2009).
68. Hou, P. et al. Pluripotent stem cells induced from mouse somatic cells by small-molecule compounds. *Science* **341**, 651–654 (2013).
69. Lapasset, L. et al. Rejuvenating senescent and centenarian human cells by reprogramming through the pluripotent state. *Genes Dev.* **25**, 2248–2253 (2011).
70. Rando, T. A. & Chang, H. Y. Aging, rejuvenation, and epigenetic reprogramming: resetting the aging clock. *Cell* **148**, 46–57 (2012).

Acknowledgements

We are thankful to Dr. Zhengfan Jiang for providing the dual-luciferase reporter assay system. We thank Dr. Shiqiang Wang and Xiaoxiao Liu for helping isolate cardiomyocytes. We also thank Dr. Xiaoyan Du and Qing Xu (Capital Medical University) for echocardiographic imaging. We thank Dr. Cheng Li for bioinformatics analysis. This work was supported by the National Natural Science Foundation of China (NSFC, Grant No. 31471205, 31171255, 91219101, 81330009, and 31671426) and the National Basic Research Program of China (973 Program, Grant No. 2013CB530700).

Author contributions

W.T. and G.L.L. conceived the project; W.T. and G.L.L. designed the experiments; G.L.L. and Y.T.G. performed the cellular and molecular experiments and analyzed the data; G.L.L. carried out the animal experiments; C.Z. contributed to all of the bioinformatics analysis; L.Z., L.S., X.K.H., L.H., X.L.T. and L.J.Z. contributed to DNA damage examination and data analysis; Z.J.Z. provided the *Zmpste24*-knockout mouse and expert assistance with data analysis; G.L.L. and W.T. wrote the manuscript.

Additional information

Supplementary Information accompanies this paper at <https://doi.org/10.1038/s41467-018-04994-z>.

Competing interests: The authors declare no competing interests.

Reprints and permission information is available online at <http://npg.nature.com/reprintsandpermissions/>

Publisher's note: Springer Nature remains neutral with regard to jurisdictional claims in published maps and institutional affiliations.



Open Access This article is licensed under a Creative Commons Attribution 4.0 International License, which permits use, sharing, adaptation, distribution and reproduction in any medium or format, as long as you give appropriate credit to the original author(s) and the source, provide a link to the Creative Commons license, and indicate if changes were made. The images or other third party material in this article are included in the article's Creative Commons license, unless indicated otherwise in a credit line to the material. If material is not included in the article's Creative Commons license and your intended use is not permitted by statutory regulation or exceeds the permitted use, you will need to obtain permission directly from the copyright holder. To view a copy of this license, visit <http://creativecommons.org/licenses/by/4.0/>.

© The Author(s) 2018